Machine Learning Algorithms for High-Resolution Gravity Prediction

Joseph O. Odumosu[1], Joe Lewis[1], Etuna Wilka Ndeunyema[1], Astrid January[1]
[1]Department of Land & Spatial Science (Geomatics Division), Namibia University of Science & Technology, Windhoek, Namibia
*Corresponding Author email: jodumosu@nust.na

(Received on 11 December 2025; In final form on 22 June 2026)

DOI: *https://doi.org/10.58825/jog.2026.20.2.309*

Abstract: Namibia's reliance on the coarse-resolution EGM2008 global geopotential model results in height conversion errors often above one meter, especially due to the lack of high-resolution terrestrial gravity data. This research analyzes Gaussian Process Regression (GPR), Support Vector Machines (SVM), Artificial Neural Networks (ANN), and Universal Kriging for the creation of high-resolution Bouguer gravity anomaly grids in the Khomas Region of Namibia. The study utilized 125 terrestrial gravity observations from the Bureau Gravimétrique International (BGI), along with SRTM elevation data and lithological density values, to train and test the models at spatial resolutions of 1.86 km and 9.26 km. Spatially Distributed Hold-Out Validation (SDHV) technique was used to check how accurate the model performed. GPR returned the best indicative accuracy (MAE = 4.67 mGal; RMSE = 5.33 mGal) and strongest agreement with Universal Kriging (r = 0.9073), while ANN exhibited overfitting tendencies at fine spatial scales and SVM produced the most conservative resolution-invariant outputs. All four techniques consistently replicated the prevailing northwest–southeast regional gravity gradient, with model divergence limited to short-wavelength spatial detail. These results show that machine learning may be used to simulate regional gravity fields and give a methodological framework to help with geoid refining and updating vertical datums in Namibia.

Keywords: Gravity prediction; Gaussian Process Regression; Support Vector Machines; Machine learning; Gravity anomalies; Geoid modeling.

1. Introduction

Gravity field modeling is crucial for geodetic applications including geoid determination, crustal deformation analysis, mass change monitoring, and vertical datum definition (Forsberg & Olesen, 2010; Gruber et al., 2012). The Earth's gravity field gives information regarding changes in subsurface density, surface topography, lithospheric structure, and dynamic processes (Blakely, 1995; Harms, 2019). As such, for Namibia to properly modernize its vertical reference system in line with the International Height Reference System (IHRS) (Ihde et al., 2017), there is need for an accurate gravity field model to serve as basis for height realization. Presently, absence of terrestrial gravity data and the need to use global models like EGM2008 make it hard to develop a high-resolution gravimetric geoid that is good for engineering-grade GNSS heighting. Global gravity models such as EGM2008, GOCE-based solutions, and satellite-only fields provide reliable long-wavelength coverage but inherently lack the spatial resolution required for precise regional modeling in rugged or geologically complex environments like Namibia (Hirt et al., 2019; Jiang et al., 2020). In numerous instances, both globally and regionally, the discrepancies between GNSS/levelling heights and EGM2008-derived orthometric heights often surpass ±1.0 m, with even greater inaccuracies observed in mountainous areas (Miky et al., 2017; Fusami et al., 2023); thus, there is a necessity for a dependable national geoid model based on high-resolution gravity data.

The absence of high-resolution and spatially continuous gravity observations causes a significant constraint in the advancement of an accurate national geoid model for Namibia. Data sparsity is a well-documented challenge in geodetic gravity field modeling, particularly in nations characterized by extensive landmasses, challenging terrain, or insufficient historical survey coverage (Basic et al., 2019; Jiang et al., 2020; Liu et al., 2024). Similar limitations have been documented throughout Africa and other developing areas, thus complicating the acquisition of gravity fields that meet contemporary geodetic precision standards (Odumosu & Nnam, 2020; Abd-Elmotaal et al., 2020).

Previously, geostatistical methods like kriging or least squares collocation (LSC) have been used to fill in gaps in gravity datasets. These methods model gravity variability mainly as a function of spatial auto-correlation (Odumosu et al., 2021). These traditional methods assume that gravity signals are second-order stationary; hence, they use spatial proximity alone to describe the covariance structure. In practice, their performance diminishes in sparsely sampled areas and in regions characterized by intricate geological and topographic variations where gravity signals diverge from solely spatial behavior (Lloyd & Atkinson, 2002; Darbeheshti & Featherstone, 2009). Odumosu et al. (2021) showed that the reliability of kriging and LSC significantly diminishes in areas characterized by an irregular station distribution or pronounced geological heterogeneity. Although GGM data improves long-wavelength content, interpolation errors persist in areas lacking near-surface

© Indian Society of Geomatics

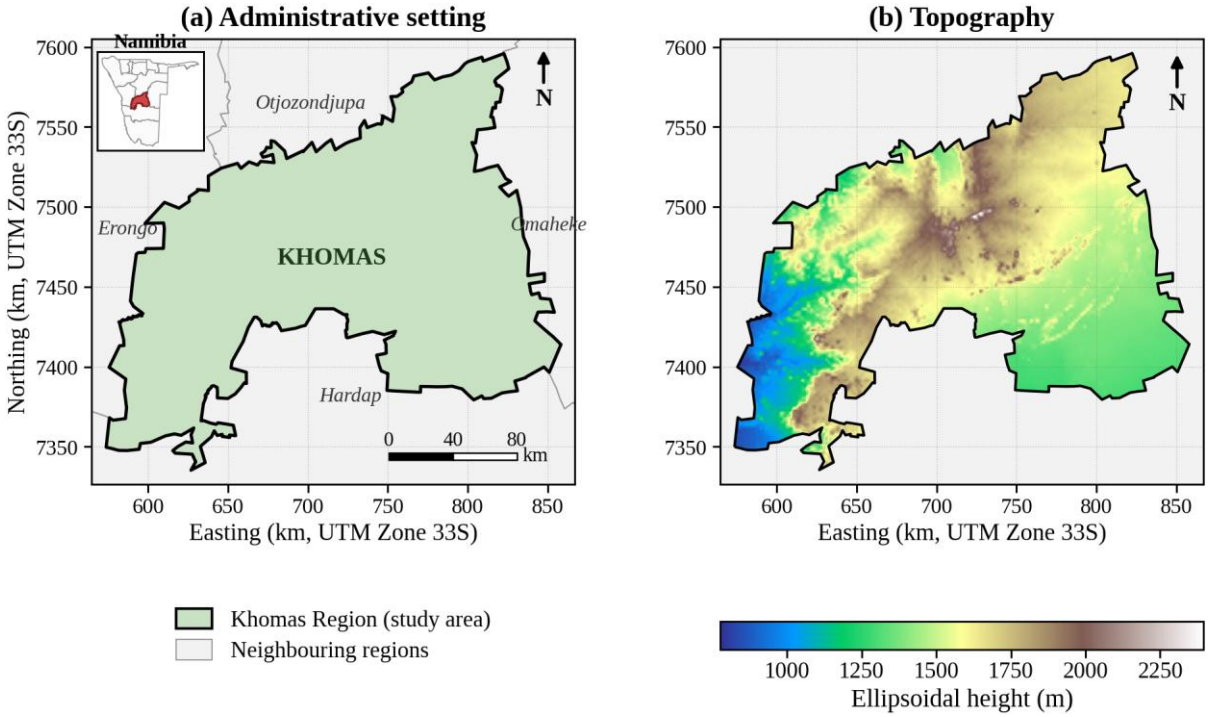


Figure 1: (a) administrative and (b) topographic maps of Khomas Region

observations. Obviously, improved prediction models must integrate geophysical information alongside distance-based covariance.

Machine learning (ML) provides a suitable alternative in which different types of predictor variables, such as station spacing, terrain elevation, slope gradients, lithology, crustal density contrasts, and even satellite-derived gravity gradients, are used to learn the non-linear structure that controls how the gravity field changes (Kaloop et al., 2022; Elshewy et al., 2024; Zanakulova et al., 2025). This differs from traditional interpolation; hence, it deduces gravity anomalies from a combination of spatial arrangement and other fundamental physical processes that affect mass distribution. Moreover, ML techniques have shown better results in geodetic and geophysical prediction tasks involving non-stationary or multifactorial relationships (Zhanakulova et al., 2025; Hu et al., 2019). Furthermore, in contrast to traditional interpolation methods, ML algorithms are more flexible (Burgess & Webster, 2019). Gaussian Process Regression has shown excellent results in geophysical time series and spatial predictions because it has an explicit covariance structure and is capable of uncertainty quantification (Moore et al., 2016). The application of machine learning to spatial prediction problems in geomatics has gained traction across Sub-Saharan Africa, where data sparsity presents a persistent operational constraint. Peprah et al. (2026) demonstrated that Random Forest and Gradient Boosting regression models outperformed classical statistical approaches for air temperature prediction in the data-sparse environment of the Greater Accra Region, Ghana, establishing a broader precedent for the utility of ML regression frameworks in African geospatial modeling contexts. The present study extends this trajectory to the domain of gravity field modeling, where analogous data scarcity challenges have similarly constrained the reliability of classical interpolation-based approaches in southern Africa.

Given Namibia's extensive gravity voids, complex lithospheric architecture, and heterogeneous topography, ML-based prediction provides a scientifically advantageous approach. It allows for the combination of spatial, geological, and topographic features, which cannot be directly integrated into kriging or LSC, thus enhancing prediction accuracy in sparsely observed areas. This study seeks to assess the efficacy of Support Vector Machines (SVM), Gaussian Process Regression (GPR), Artificial Neural Networks (ANN), and Universal Kriging for gravity prediction across Khomas region of Namibia by combining available terrestrial measurements obtained from the Bureau Gravimétrique International (BGI), elevation differences obtained from the Shuttle Radar Topographic Mission (SRTM), and geological density information from the Ministry of Mines and Energy of Namibia. Using the identified methods, high-resolution gravity anomaly grids were generated and independently assessed using a Spatially Distributed Hold-Out Validation (SDHV) method, in which four geographically representative points are withheld from training and used exclusively for testing, to examine predictive accuracy and relative model performance.

2. Study area

The study was conducted in the Khomas Region of central Namibia (Figure 1). The region is characterized by intricate topography, steep escarpment landscapes, and considerable elevation variability associated with basement uplifts and erosion surfaces. It lies within the southern extent of the Damara Orogenic Belt, where strong lateral variations in crustal density and tectonic structures give rise to significant spatial fluctuations in the gravity field. Also, surface elevation varies widely across short horizontal distances, and geological units range from high-density metamorphic formations to lower-density sedimentary rocks. These conditions produce short-

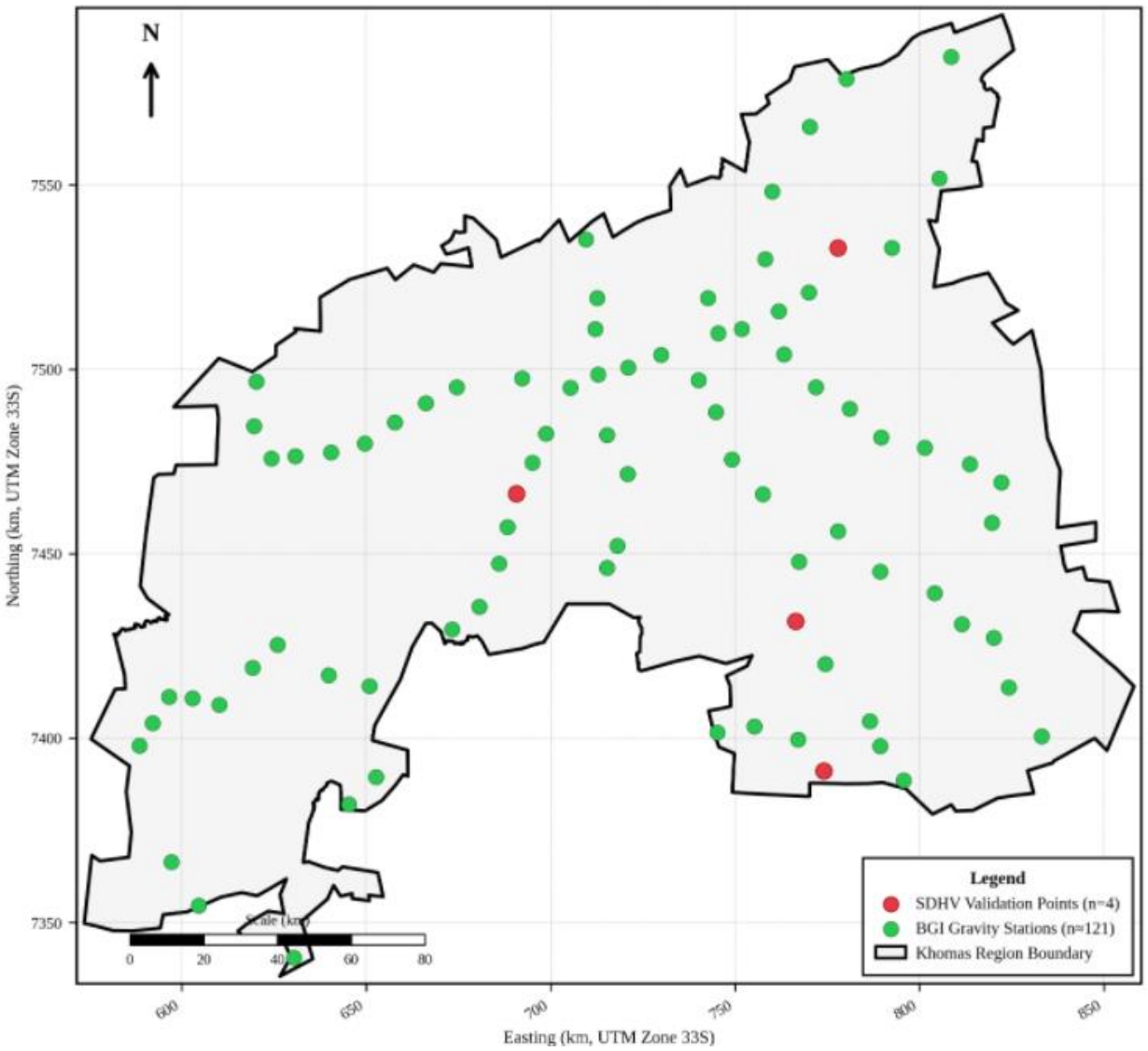


Figure 2: Spatial distribution of BGI gravity validation and test data points within the Khomas Region

wavelength gravity anomalies that require fine-scale predictive modeling for realistic representation, making the region a particularly demanding and informative test environment for the methods evaluated in this study.

Till date, Khomas region remains severely data-limited, with sparse and uneven terrestrial gravity coverage and minimal nationwide modernization of gravity infrastructure. Reliance on global gravity models such as EGM2008 results in height conversion errors frequently exceeding one meter, which is not suitable for engineering, GNSS height modernization, infrastructure planning, and crustal studies (Miky et al., 2017; Fusami et al., 2023). Satellite-based solutions provide adequate long-wavelength information but do not resolve localized anomalies induced by terrain gradients and rapid geological transitions. As a result of these issues (rugged terrain, nonuniform data distribution, need for sub-decimeter or even sub-centimeter vertical control, etc), there is need for an all-inclusive and robust predictive modeling approach that is capable of inferring realistic short-wavelength gravity variations from limited measurements. Machine learning provides a pathway to realizing such and also generating improved gravity estimates suitable for national geodetic modernization.

3. Materials and Methods

3.1 Data Sources and Materials

This study employed a regional gravity dataset consisting of 125 terrestrial Bouguer gravity anomaly observations for the Khomas Region of Namibia, sourced from the BGI. The observations consist of sparse yet high-quality point measurements referenced to the zero-tide system, functioning as the principal dependent variable for model development (Figure 2). The linear spatial pattern of the BGI data points reflects the survey track lines characteristic of regional gravity campaigns, in which observations are collected along traverses rather than as random point distributions. Metadata relating to the accuracies of the 125 BGI gravity data points was not available from the source. Nevertheless, regional terrestrial gravity surveys are mostly performed with relative gravimeters with field repeatability exceeding 0.2 mGal and final network accuracies typically ranging from 0.1 to 0.5 mGal (Sobrero, 2024). For this reason, similar assumptions were made about the given data. In order to

Table 1: Descriptive statistics of the training dataset (n = 121), Khomas Region, Namibia

Attribute	Min	Max	Mean	Standard Deviation	Range
UTM Easting X (m)	578981.607	844289.830	730816.950	74187.023	265308.223
UTM Northing Y (m)	7351693.120	7583474.610	7457705.200	48983.567	231781.490
Elevation (m)	825.032	2040.740	1533.835	223.936	1215.708
Density (g/cm³)	1.600	2.900	2.055	0.419	1.300
Gravity Anomaly (mGal)	-11.419	96.878	44.036	21.171	108.296

Note that all planimetry coordinates are specified in UTM Zone 33S (WGS 84 ellipsoid)

improve the predictive accuracy and illustrate geophysical influences on the gravity field, supplementary geospatial datasets were integrated. The supplementary dataset were topographic data derived from the Shuttle Radar Topography Mission (SRTM) 30-meter resolution Digital Elevation Model (DEM). Following the digital terrain analysis principles in Warren et al. (2004) and Xiong et al. (2022), elevation and slope were derived from the DEM as topographic and geomorphometric variables. Furthermore, geological context was added to the dataset using regional lithological maps obtained from the Ministry of Mines and Energy of Namibia. This is similar to how gravity-based crustal studies work (Ikirri et al., 2023). Finally, the density values were assigned to each gravity observation point based on the most common lithological unit that was mapped at or near that point.

The Khomas Region has metamorphic basement rocks, calcareous sequences, and sedimentary cover units. The average bulk densities of these units range from about 1.6 g/cm³ for unconsolidated sediments to 2.9 g/cm³ for high-grade metamorphic rocks, which is in line with standard petrophysical compilations for the Damara Orogenic Belt. Although density assignment from geological maps entails intrinsic spatial uncertainty that is generally estimated at ±0.1–0.2 g/cm³, depending on lithological heterogeneity and map scale, this uncertainty was not formally propagated through the models. Following the direct relationship between subsurface mass distribution and Bouguer gravity anomalies (density being a fundamental parameter in the Bouguer reduction itself), density variation becomes an important predictor variable, as already shown in previous studies (Ikirri et al., 2023). The training dataset's density values ranged from 1.6 to 2.9 g/cm³, with an average of 2.06 g/cm³ (Table 1). This shows that the study area has a mix of rock types. The WGS-84 reference ellipsoid was used to resample and georeference all of the datasets to a common spatial framework.

All predictor variables (elevation, slope, lithological density values, and terrestrial gravity observations) were extracted from their respective datasets, standardized to a common spatial resolution, and assembled into a unified modeling dataset. Continuous variables were normalized to zero mean and unit variance to ensure comparability across predictors of differing scales and units. The resulting database comprised a fully structured input matrix in which elevation, slope, and density attributes served as predictor variables, with Bouguer gravity anomalies defined as the target variable for machine learning model training.

3.2 Modeling Approach

Four predictive modeling approaches were evaluated for high-resolution gravity field estimation. The models were Gaussian Process Regression (GPR), Support Vector Machines (SVM), Artificial Neural Networks (ANN), and Universal Kriging. These models represent both traditional geostatistical interpolation and modern machine learning approaches (Hu et al., 2019; Zhanakulova et al., 2025).

GPR was implemented using a Matérn covariance kernel, which allows for efficient modelling of model spatial processes with different levels of roughness. The Matérn covariance kernel has been used in past studies for geodetic prediction problems with sparse datasets (Moore et al., 2016). The model calculates the posterior mean and covariance of the gravity field based on the data that has been observed; hence, it makes it possible to interpolate and measure prediction uncertainty at the same time.

The SVM used a radial basis function (RBF) kernel, which implicitly maps input variables into a high-dimensional feature space via the kernel trick. This helps to model nonlinear relationships between the predictor variables and the target gravity anomalies. Grid-search cross-validation was used to optimize hyperparameters (the regularization parameter and kernel width). This ensures model stability and generalization.

Backpropagation was used to train ANN as a multilayer perceptron with one hidden layer. The ANN was used to model complicated nonlinear relationships between inputs and outputs. Because it is sensitive to the amount of data and how the weights are set up at the start, a systematic grid-search method was used to find the best values for architecture parameters like the neuron count and the learning rate; hence, maximizing prediction accuracy on the training dataset.

Universal Kriging served as the geostatistical benchmark, applying a polynomial drift function to account for large-scale spatial trends in the gravity field, combined with semi-variogram analysis to model the residual spatial auto-correlation structure. The gravity anomaly observations were fitted with a spherical variogram model, and the covariance structure was used to interpolate anomaly values at unmeasured grid locations.

3.3 Model Evaluation and Spatially Distributed Hold-Out Validation (SDHV)

Spatially Distributed Hold-Out Validation (SDHV) strategy was used to test the model's performance. This method is suitable for gravity field studies with few

Table 2: Coordinates and gravity anomaly values of the four spatially distributed hold-out validation points

Point ID	X (m)	Y (m)	Elevation (m)	Density (g/cm³)	Gravity Anomaly (mgal)
A14	780178.578	7399006.699	1310.670	1.780	33.517
A46	771509.045	7437219.991	1419.030	1.780	58.794
A69	689958.459	7469124.127	1837.060	2.700	70.004
A117	784556.680	7532471.018	1610.000	1.800	27.065

terrestrial observations. In this method, four points that were well spread out across the study area were left out of the training data set and only used for independent validation. The other 121 observations were used to train the model. The four validation points were chosen to provide a good range of geological and topographic conditions in the area, so that the model's predictions could be tested in all of them. This method was chosen over full Leave-One-Out Cross Validation (LOOCV) because it keeps a larger, more stable training set and allows for independent spatial testing at places that are representative of the area. It is acknowledged that performance statistics obtained from four validation points yield indicative rather than conclusive model rankings; as such, the reported metrics are interpreted in this context. For future work, larger validation datasets shall be used to provide statistically sound model rankings.

Two complementary performance indicators, Root Mean Square Error (RMSE) and Mean Absolute Error (MAE), were used to quantify the prediction accuracy. RMSE gives greater weight to large individual prediction errors due to the squaring operation, making it sensitive to outlying residuals, while MAE provides an equal-weighted measure of average prediction deviation. These metrics were used as a consistent basis for comparing the performance of Gaussian Process Regression, Support Vector Machines, Artificial Neural Networks, and Universal Kriging across the hold-out validation points.

3.4 Spatial Prediction and Grid Generation

Finally, each model was used to predict gravity data across continuous spatial grids at resolutions of 1.86 km and 9.26 km to cover the full extent of the study area. Residual filtering and surface continuity checks were applied to the predicted grids to ensure geophysically meaningful spatial gradients and to suppress unrealistic oscillations in areas with sparse observational control. Model outputs were compiled into gravity anomaly maps and assessed both visually and numerically, with spatial patterns interpreted in the context of the known regional tectonic framework of the Khomas Region, as described in Section 2. Consequently, the resulting surfaces represent some of the initial machine learning-derived high-resolution gravity field estimates for the study area, as there has been very limited documented earlier research conducted within the study area. Hence, the results presented herein provide a basis for potential integration into future geoid modeling and national vertical datum modernization efforts.

4. Results

A total of 125 terrestrial Bouguer gravity anomaly observations obtained from BGI were used in this study. Following data preparation, 121 observations served as the training set, while four spatially distributed independent points (Table 2) were withheld for SDHV validation. Each point included UTM coordinates (X and Y), ellipsoidal height, lithological density value, and Bouguer gravity anomaly, the latter derived through the standard reduction procedure comprising normal gravity computation via the Somigliana formula, Free-Air correction, and Bouguer plate correction referenced to the WGS-84 ellipsoid. Table 1 summarizes key statistics for the training data, which cover elevations from 825.03 to 2,040.74 m and Bouguer gravity anomalies ranging from –11.42 to 96.88 mGal.

4.1 Gravity Prediction Using Machine Learning and Kriging

Four prediction models were developed accordingly using two different grid resolutions over the study area in the Khomas Region. The first was a small grid with 10,670 cells spaced 1.86 km apart for precise spatial analysis. The second was a larger grid with 432 cells spaced 9.26 km apart for regional interpretation.

4.1.1 Artificial Neural Network (ANN)

The predictions made by the ANN model had the widest dynamic range of all the models. At a resolution of 1.86 km, projected values varied from –67.56 mGal to 148.95 mGal (Table 3), significantly surpassing the observed training data range of –11.42 to 96.88 mGal at both ends. This range, which is about 56 mGal below and 52 mGal over the observed limits is indicative of overfitting rather than a real geophysical signal. This is consistent with known sensitivity of ANN to training data that is sparse and unevenly distributed. It is important to be careful when

Table 3: Descriptive statistics of ANN-predicted Bouguer gravity anomalies across the Khomas Region at two spatial resolutions (fine-scale of 1.86 km grid

	1.86km grid	9.26km grid
Parameter	Value (mGal)	Value (mGal)
Minimum	-67.563	-7.366
Maximum	148.952	94.211
Range	216.515	101.577
Standard Deviation	24.282	18.986
Mean	39.214	41.234

interpreting predicted values that are beyond the range of observed training data, especially in regions with sparse datasets.

At the coarser resolution, the predicted range contracted by 53% to 101.58 mGal, falling within the observed data range of 108.30 mGal and with individual predicted values confined between –7.37 and 94.21 mGal, both within the observed training bounds. This suggests that spatial aggregation at the coarser resolution effectively eliminates the extrapolation tendency observed at the finer scale, although this comes at the cost of suppressing short-wavelength spatial detail.

4.1.2 Gaussian Process Regression (GPR)

GPR produced the most stable predictions across all resolutions. At a resolution of 1.86 km, the projected anomalies varied from –7.13 to 91.02 mGal (Table 4), and they stayed completely within the observed training data ranges of –11.42 to 96.88 mGal. At 9.26 km resolution, the forecast range changed slightly (93.19 mGal), and the mean and standard deviation stayed almost the same across all scales (≈42.4 mGal and 16–17 mGal, respectively). This stability across resolutions is due to GPR's covariance-driven probabilistic formulation. In this formulation, the Matérn kernel and Bayesian posterior mean automatically control spatial oscillations and keep predictions within physically realistic limits. These characteristics suggest that GPR may be particularly well suited for geodetic applications in data-sparse environments where prediction consistency and physical plausibility across spatial scales are important requirements.

Table 4: Descriptive statistics of GPR-predicted Bouguer gravity anomalies across the Khomas Region at two spatial resolutions (fine-scale of 1.86 km grid spacing)

	1.86km grid	9.26km grid
Parameter	**Value (mGal)**	**Value (mGal)**
Minimum	-7.126	-4.284
Maximum	91.016	88.906
Range	98.142	93.189
Standard Deviation	16.627	17.109
Mean	42.376	42.368

4.1.3 Support Vector Machines (SVM)

SVM produced the most conservative predictions among all four models. At 1.86 km resolution, predicted values ranged from 0.80 to 83.36 mGal (Table 5), well within the observed training data range of –11.42 to 96.88 mGal. The prediction range changed negligibly between resolutions (82.57 mGal at 1.86 km and 83.10 mGal at 9.26 km), and both the mean (≈43.4 mGal) and standard deviation (≈14.0–14.3 mGal) remained virtually unchanged across scales. This shows a strong regularization inherent in the SVM margin-based optimization.

Notably, SVM produced no negative predictions at either resolution, despite the observed data containing negative anomalies as low as –11.42 mGal. This indicates that the model's conservative generalization behavior suppresses the lower end of the anomaly spectrum and underrepresents the full dynamic range of the gravity field. Furthermore, the standard deviation of approximately 14 mGal falls considerably short of the standard deviation of the original data (21.17 mGal). Although this might be considered a strength of SVM, making it well suited for regional mapping where spatial smoothness and numerical stability are priorities, it suggests the model may inadequately resolve short-wavelength negative anomalies in geologically complex settings.

Table 5: Descriptive statistics of SVM-predicted Bouguer gravity anomalies across the Khomas Region at two spatial resolutions (fine-scale of 1.86 km grid spacing, and regional-scale of 9.26 km grid spacing)

	1.86km grid	9.26km grid
Parameter	**Value (mGal)**	**Value (mGal)**
Minimum	0.797	0.169
Maximum	83.363	83.264
Range	82.566	83.095
Standard Deviation	13.988	14.299
Mean	43.403	43.432

4.1.4 Universal Kriging (UK)

Table 6: Descriptive statistics of UK-predicted Bouguer gravity anomalies across the Khomas Region at two spatial resolutions (fine-scale of 1.86 km grid spacing and regional-scale of 9.26 km grid spacing)

	1.86km grid	9.26km grid
Parameter	**Value (mGal)**	**Value (mGal)**
Minumum	-9.434	-6.691
Maximum	88.434	88.392
Range	97.868	95.082
Standard Deviation	19.196	19.358
Mean	40.828	40.996

Universal Kriging produced predictions that most closely reproduced the statistical distribution of the observed training data. At 1.86 km resolution, predicted anomalies ranged from –9.43 to 88.43 mGal (Table 6), remaining within the observed data bounds and capturing negative anomalies consistent with the lower end of the observed range. The prediction range of 97.87 mGal at fine resolution and 95.08 mGal at coarse resolution closely approximates the observed span of 108.30 mGal, and the standard deviation of approximately 19.2 mGal is the closest of all models to the observed value of 21.17 mGal. The mean gravity value (≈40.8–41.0 mGal) is marginally

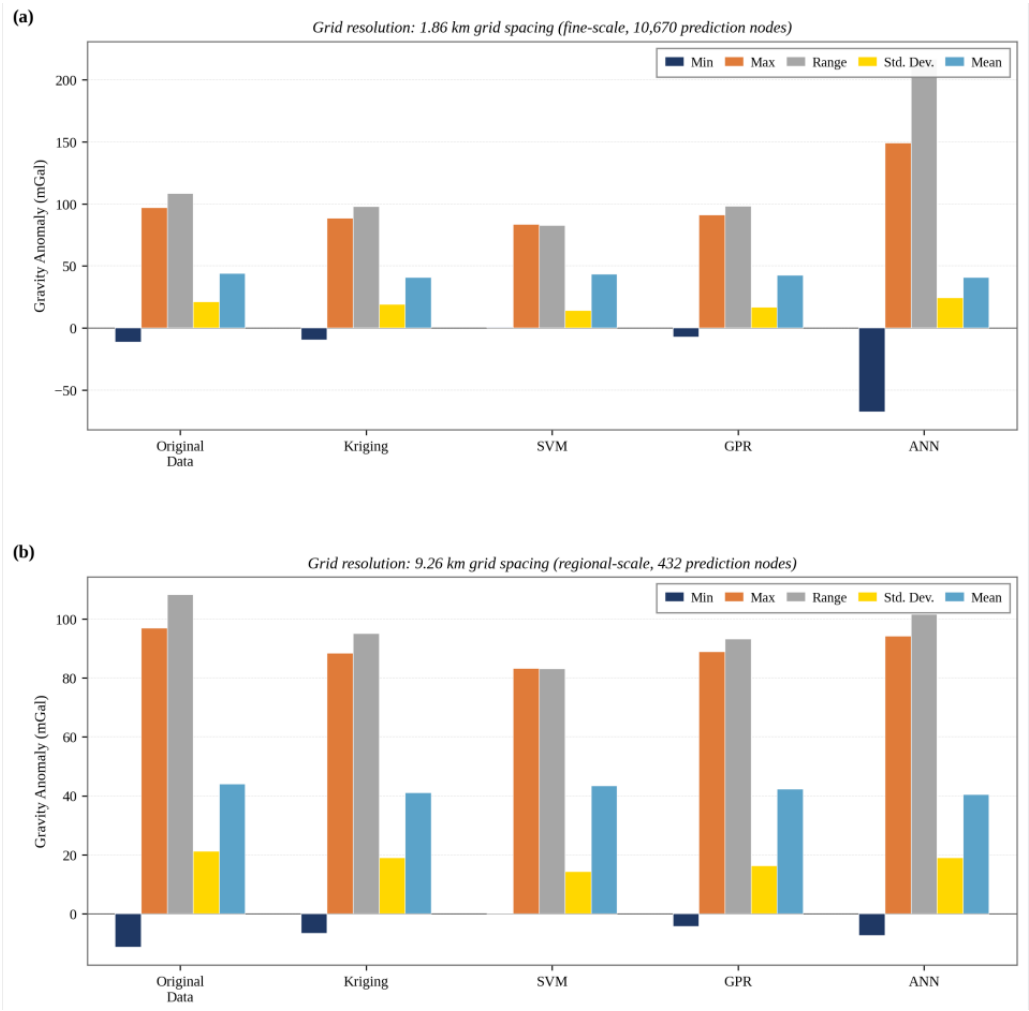


Figure 3: Comparative bar charts of minimum, maximum, range, standard deviation, and mean values for the original dataset and prediction models at (a) 1.86 km and (b) 9.26 km spatial resolutions.

lower than the observed mean of 44.04 mGal. This is consistent with the smoothing effect of the fitted variogram model, as it tends to pull predictions toward the global mean in areas distant from observations. This slight difference in range and standard deviation between resolutions shows that Universal Kriging is naturally resistant to changes in variability caused by resolution. This is because the semi-variogram encodes the spatial auto-correlation structure. Being the geostatistical benchmark, these results confirm that Universal Kriging provides a statistically faithful representation of the observed gravity field distribution, though its inability to incorporate auxiliary predictors such as elevation and density limits its capacity to resolve physically motivated short-wavelength signals beyond what spatial proximity alone can support.

4.2 Comparative assessment of Prediction models

A comparative analysis of the four modeling approaches was carried out by examining the statistical descriptors (minimum, maximum, range, standard deviation, and mean) that were derived from model outputs at both grid resolutions (1.86 km and 9.26 km) against the corresponding statistics of the original observed datasets. The results, presented in Tables 7 and 8, provide a basis for assessing how each model reproduces the statistical distribution and dynamic range of the observed Bouguer gravity anomaly field across spatial scales.

Given that the observed dataset had a dynamic range of 108.30 mGal (–11.42 to 96.88 mGal) and a standard deviation of 21.17 mGal, the four models exhibited notably different behavior at the finer spatial resolution of 1.86 km. The statistical descriptors of each model output relative to the original data are summarized in Tables 7 and 8 and illustrated in Figures 3(a) and 3(b). Among the models, ANN produced the widest prediction range of 216.51 mGal, extending approximately 56 mGal below and 52 mGal above the observed data limits. This substantial excess in the observed bounds primarily suggests overfitting, caused by the model's response to noise and local irregularities in the sparse training data, and not necessarily an underlying geophysical signal. Also, ANN's standard deviation of 24.28 mGal exceeds the observed value of 21.17 mGal (approximately a 15% increase). This further confirms a tendency of excessive variability at fine spatial scales.

The prediction ranges for GPR and Universal Kriging were 98.14 mGal and 97.87 mGal, respectively. Both of these values were about 10 mGal lower than the observed dataset range of 108.30 mGal, representing an underestimation of about 9–10%. GPR's standard deviation of 16.63 mGal is around 21% lower than the observed value of 21.17 mGal.

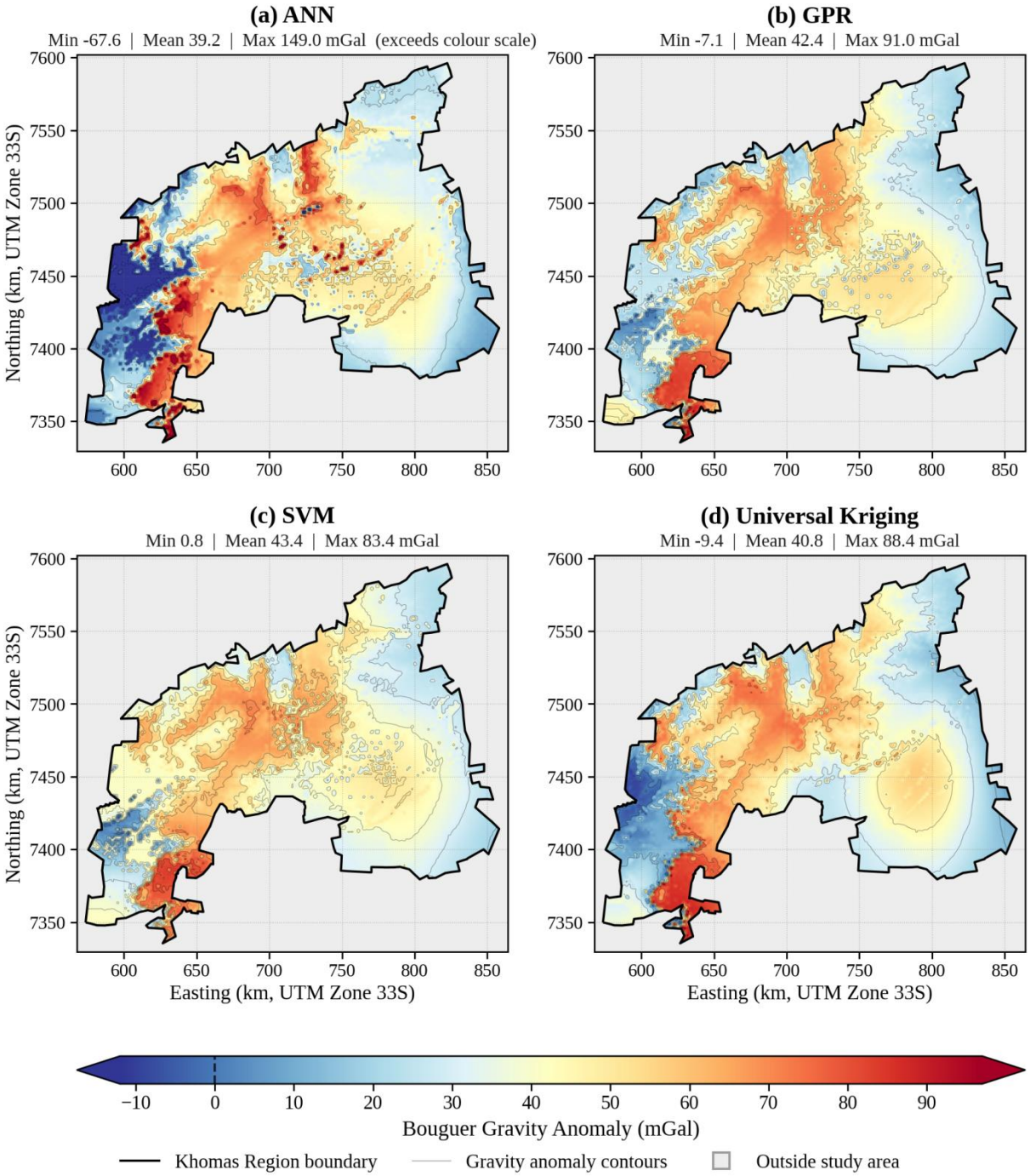


Figure 4: Predicted Bouguer gravity anomaly maps at 1.86km grid from (a) ANN (b) GPR (c) SVM (d) Kriging

This means that GPR avoids the extreme oscillations that ANN shows, but it does reduce the entire spatial variability of the gravity field to some extent. Universal Kriging had a mean of 40.83 mGal, which was 4.04 mGal higher than the observed mean, and a standard deviation of 19.20 mGal, which was the closest of all the models to the observed value. This is attributed to the fitted variogram model's smoothing, which gives more weight to predictions that are farther away from the data. This explains why the mean field is consistently underestimated.

SVM generated the narrowest prediction range (82.57 mGal) and the lowest standard deviation (13.99 mGal) among all models. It shows an underestimation of the observed range and standard deviation by approximately 24% and 34%, respectively. The absence of negative predictions, despite negative anomalies being present in the observed data, also shows the model's conservative generalization behaviour rather than a deliberate feature of its optimization. While this conservatism produces numerically stable outputs, it results in an under-representation of the lower end of the observed anomaly spectrum and suppresses spatial gradients that may carry geophysical significance.

At the coarser resolution of 9.26 km, the prediction ranges for most models become slightly smaller. This is a result of the natural smoothing effect of spatial aggregation. Nevertheless, it exhibited the biggest drop as the prediction range shrank by 53% from 216.51 mGal to 101.58 mGal, with each predicted value within the range of the observed

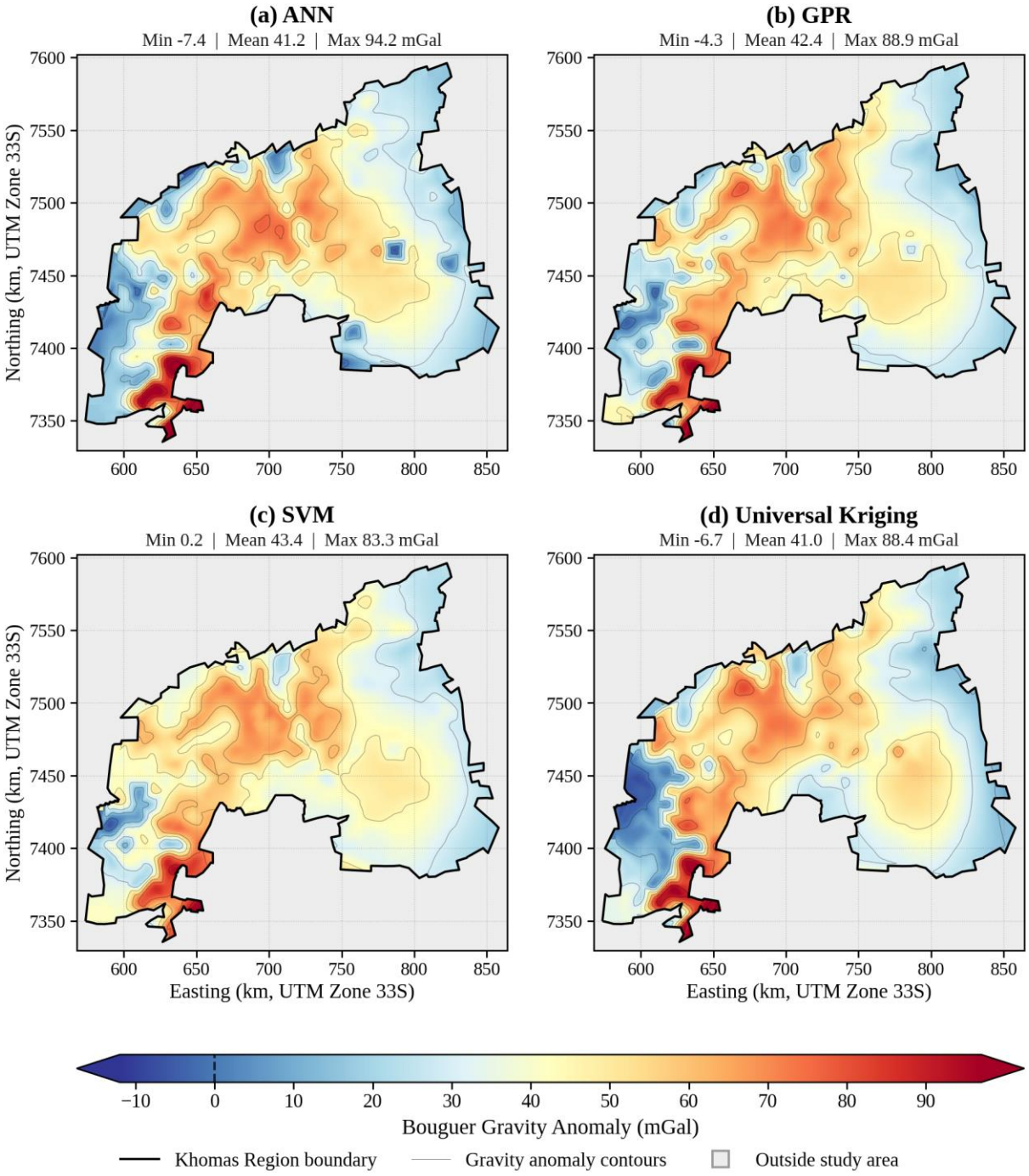


Figure 5: Predicted gravity anomaly maps at 9.26 km grid from (a) ANN (b) GPR (c) SVM (d) Kriging

data. This considerable resolution sensitivity demonstrates that ANN's fine-scale predictions are significantly affected by high-frequency responses to local input fluctuations, many of which are diminished when spatial aggregation is utilized.

GPR and Universal Kriging again showed very stable behavior throughout resolutions. At the coarser resolution, they had ranges of 93.19 mGal and 95.08 mGal, respectively, and both stayed close to their fine-scale values and within the range of the observed data. This consistency suggests that both methods preserve regional spatial gradients effectively and are resistant to resolution-induced variability changes. SVM also showed very little variation between resolutions (82.57 vs. 83.10 mGal), and the standard deviation remained the same at about 14.30 mGal. This further supports it being the most conservative and resolution-invariant model with respect to anomaly spread.

4.3 Model Validation Performance

Model performance (Table 9) was assessed using spatially distributed hold-out validation (SDHV) against the four independent test points. Given that only four validation points were available, the reported metrics serve basically as indicative of relative model behavior rather than as definitive accuracy rankings. With this noted, GPR returned the lowest error metrics among the four models (MAE = 4.67 mGal; RMSE = 5.33 mGal). SVM followed closely, with a MAE difference of only 0.21 mGal and an RMSE difference of 0.67 mGal relative to GPR (MAE = 4.88 mGal; RMSE = 6.00 mGal). This means that the two

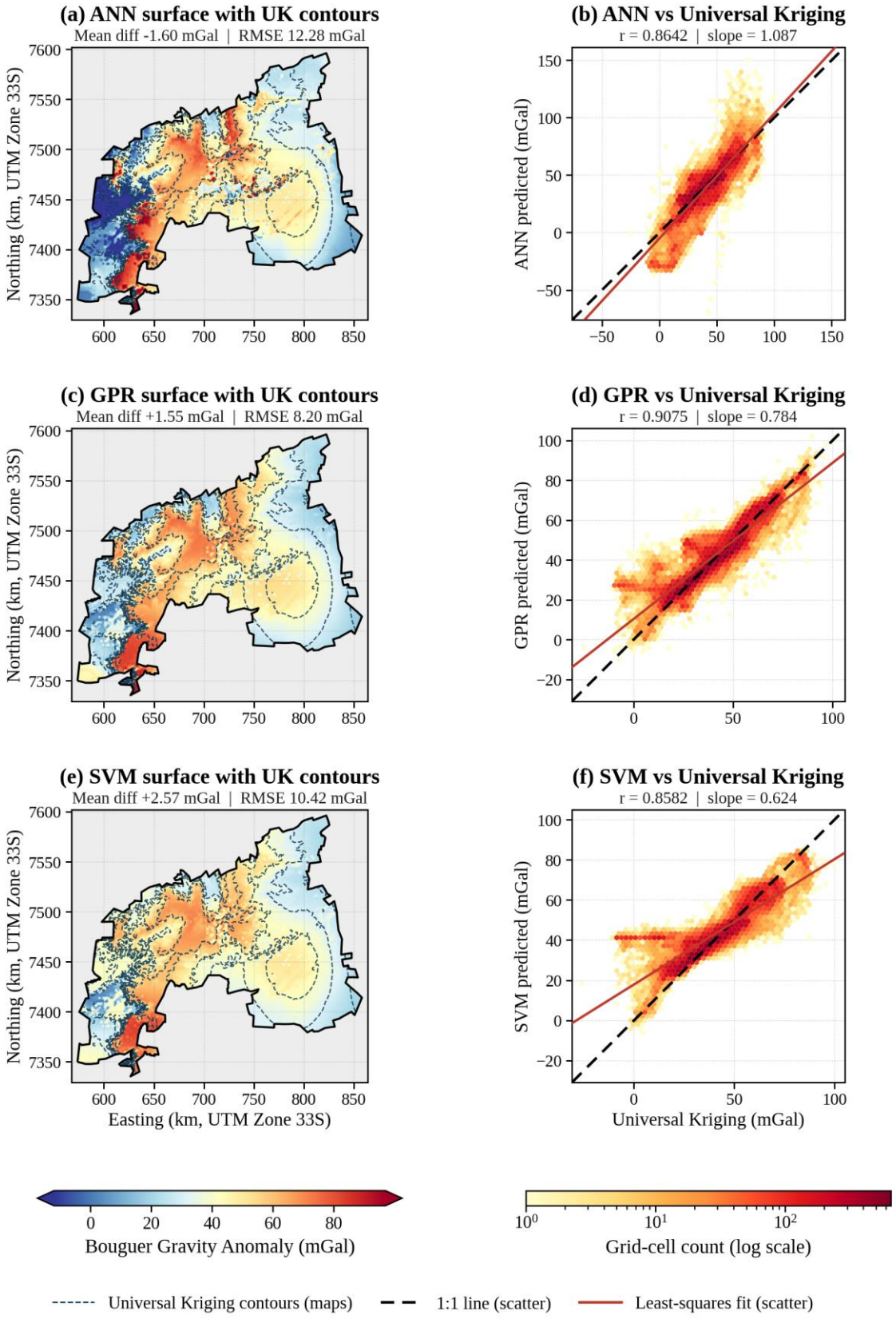


Figure 6: Spatial auto-correlation between ML models and Universal Kriging @ 1.86 km resolution

models generally show similar predictive performance. The ANN resulted in higher residuals (MAE = 5.48 mGal; RMSE = 7.54 mGal), which is consistent with its tendency for localized overfitting at fine spatial scales for sparse training data. Universal Kriging returned the highest residuals (MAE = 7.25 mGal; RMSE = 7.81 mGal), reflecting its systematic tendency to under-predict at higher anomaly values. This is a known consequence of variogram-driven spatial smoothing that pulls predictions toward the global mean in areas of limited observational support.

Looking at the residuals for each validation point (Table 10) shows that the model makes predictions in different

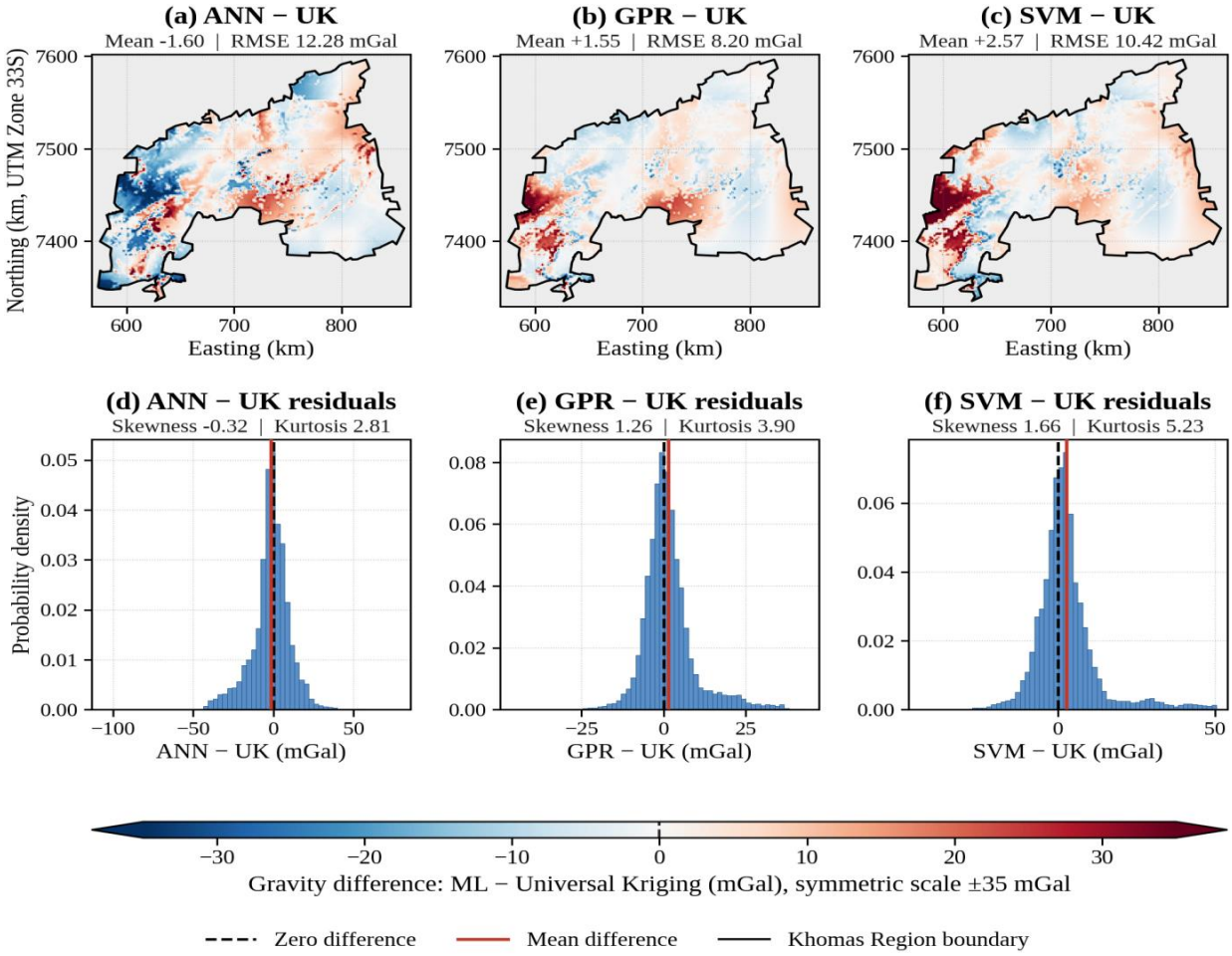


Figure 7: Spatial difference maps and residual distributions between machine learning model predictions and Universal Kriging (UK): (a) ANN − UK, (b) GPR − UK, (c) SVM − UK, and corresponding residual histograms in panels (d–f)

ways. GPR made the most accurate prediction at Point 14 (residual −0.40 mGal), but consistently underpredicted at the other three points, with residuals of −7.23, −5.72, and −5.33 mGal at Points 46, 69, and 117, respectively (Table 10). The fact that it is consistently negative suggests that the Bayesian posterior mean of the GPR may be biased toward lower values in regions with little empirical support. ANN did a decent job at three sites with residuals of ±2.70 mGal but significantly underestimated at Point 46 by 14.45 mGal. This was the largest individual residual recorded in all models and validation points. This is consistent with its known tendency to overfit at fine spatial scales. Universal Kriging consistently underpredicted at all four validation points, with residuals of +2.45, −9.66, −7.43, and −9.46 mGal at Points 14, 46, 69, and 117, respectively. This is because the variogram-driven smoothing tendency drags predictions toward the global mean. The SVM residuals ranged from +2.11 to −10.72 mGal, with two of the four absolute residuals being less than 4.43 mGal. It is worth mentioning that SVM overestimated at Point 14 (+2.11 mGal) and underestimated at the other three points. This indicates a small direction mismatch. Three of the four residuals were less than 4.43 mGal. However, it overestimated significantly at Point 46 by 10.72 mGal which shows that all models had difficulties at this position.

All models encountered difficulty at Point 46, with underestimations of 14.45 mGal (ANN), 10.72 mGal (SVM), 9.66 mGal (Kriging), and 7.23 mGal (GPR). This suggests that the particular location may represent a geophysically complex zone that is inadequately constrained by the surrounding training observations. Overall, GPR demonstrated the most consistent residuals across the four validation points, with a spread of only 6.83 mGal (−0.40 to −7.23 mGal), reflecting stable prediction behavior under the sparse observational conditions of the study area.

4.4 Spatial Prediction Results

All four models broadly captured the major gravity anomaly patterns observed across the Khomas Region, including high anomalies concentrated in the western and central domains, lower anomalies toward the east, and a northwest–southeast gradient broadly consistent with the known regional tectonic framework. At 1.86 km resolution, spatial outputs preserved short-wavelength variations and sharper spatial gradients (Figure 4), while the 9.26 km grids (Figure 5) captured regional-scale gradients with reduced high-frequency variability. ANN exhibited the largest compression of dynamic range when grid resolution was coarsened, with a 53% reduction from 216.51 mGal to 101.58 mGal (Table 11), consistent with

Table 7: Model performance in relation to original data at 1.86km

1.86km grid					
Parameter	**ANN**	**GPR**	**SVM**	**Kriging**	**Original data**
Minimum	-67.563	-7.126	0.797	-9.434	-11.419
Maximum	148.952	91.016	83.363	88.434	96.878
Range	216.515	98.142	82.566	97.868	108.296
Standard Deviation	24.282	16.627	13.988	19.196	21.171
Mean	39.214	42.376	43.403	40.828	44.036

Table 8: Model performance in relation to original data at 9.26km

9.26km grid					
Parameter	**ANN**	**GPR**	**SVM**	**Kriging**	**Original data**
Minimum	-7.366	-4.284	0.169	-6.691	-11.419
Maximum	94.211	88.906	83.264	88.392	96.878
Range	101.577	93.189	83.095	95.082	108.296
Standard Deviation	18.986	17.109	14.299	19.358	21.171
Mean	41.234	42.368	43.432	40.996	44.036

its established sensitivity to fine-scale input variations. In contrast, GPR, SVM, and Universal Kriging showed minimal range changes across resolutions, with variations of less than 2 mGal in all cases (Table 11), confirming their resolution-invariant spatial behaviour.

The gravity anomaly maps generated at both spatial resolutions (Figures 4 and 5) confirm that all four modeling approaches reproduced the dominant regional gravity field pattern across the Khomas Region. In all cases, high-magnitude Bouguer anomalies are consistently concentrated in the western and central domains, while lower values characterize the eastern sector, producing a persistent northwest–southeast gradient broadly consistent with the known tectonic framework of the Damara Orogenic Belt. This agreement across methods, despite their fundamentally different mathematical formulations, indicates that the primary large-scale signal is robustly captured regardless of model choice.

Differences among the methods are most apparent at the 1.86 km resolution, where model-specific spatial behavior is clearly expressed. ANN produced the broadest anomaly range and the most spatially variable output, with sharp local transitions and prediction values extending beyond the observed data bounds. This behavior is attributed to the overfitting tendency identified in the quantitative analysis. GPR produced smoother and more spatially stable distributions. The probabilistic formulation of GPR based on covariance limited the predictions to the physically plausible range and preserved the regional gradient structure. The spatial outputs obtained by Universal Kriging were statistically similar to GPR in terms of range and standard deviation, with a moderate spatial variability controlled by the fitted semivariogram structure. Nonetheless, its output is noticeably smoother in zones distant from observation points due to the mean-regression effect of the variogram model. Finally, SVM produced the smoothest anomaly surfaces with the narrowest dynamic range across the study area, with no negative predictions despite negative anomalies being present in the observed data. This reflects its conservative generalization behavior and underrepresentation of the lower end of the anomaly spectrum.

Table 9: Model performance based on SDHV (four spatially distributed hold-out points)

Model	**MAE (mGal)**	**RMSE (mGal)**	**Rank**
GPR	4.67	5.33	1
SVM	4.88	6.00	2
ANN	5.48	7.54	3
Kriging	7.25	7.81	4

At the coarser resolution of 9.26 km, differences among the models diminish considerably. ANN converges toward the observed data range as the spatial aggregation suppresses fine-scale high-frequency responses, while GPR, SVM, and Universal Kriging show minimal change from their fine-scale outputs. This confirms their inherent resistance to resolution-induced variability changes. At this scale, the four models produce broadly similar regional patterns, suggesting that model selection becomes less critical when the primary objective is large-scale regional gravity field characterization.

4.5 Discussion of Results

4.5.1 Spatial auto-correlation

Figure 6 shows the spatial autocorrelation analysis, which indicates that all three ML models and Universal Kriging agree strongly across the Khomas Region. GPR has the closest correlation (r = 0.9073), followed by ANN (r = 0.8644) and SVM (r = 0.8581) at a resolution of 1.86 km.

Table 10: Predicted Bouguer gravity anomalies and their residuals (Predicted − Observed) at the four SDHV hold-out validation points (mGal).

Point ID	Observed	ANN	ANN Residual	GPR	GPR Residual	SVM	SVM Residual	UK	UK Residual
A14	33.52	30.82	−2.70	33.12	−0.40	35.63	2.11	35.97	2.45
A46	58.79	44.34	−14.45	51.56	−7.23	48.07	−10.72	49.13	−9.66
A69	70	67.35	−2.65	64.28	−5.72	65.57	−4.43	62.57	−7.43
A117	27.06	29.17	2.11	21.73	−5.33	24.79	−2.27	17.6	−9.46

Table 11: Dynamic range comparison across spatial resolutions

Model	1.86 km Grid			9.26 km Grid			Range Change		Interpretation
	Min (mGal)	Max (mGal)	Range (mGal)	Min (mGal)	Max (mGal)	Range (mGal)	Δ Range (mGal)	Δ Range (%)	
ANN	-67.56	148.95	216.51	-7.37	94.21	101.58	114.93	-53.1%	Large range shrinkage at coarse resolution
GPR	-7.13	91.02	98.14	-4.28	88.91	93.19	4.95	-5.0%	Ranges within observed data bounds
SVM	0.80	83.36	82.57	0.17	83.26	83.10	0.53	+0.6%	Most resolution-invariant model
Kriging	-9.43	88.43	97.87	-6.69	88.39	95.08	2.79	-2.9%	Range closely approximates observed data
Observed	-11.42	96.88	108.30	—	—	—	—	—	(BGI terrestrial Bouguer anomalies)

The regression slope for GPR was closest to one, and the predicted values were most closely grouped around the 1:1 line. This supports its established role as the most reliable predictor in this investigation. These correlation magnitudes are consistent with what Kaloop et al. (2022) and Zhanakulova et al. (2025) found.

This is consistent with past literature, which showed strong agreement between ML and geostatistical models when predicting regional gravity, especially when shared input predictors anchor the large-scale signal structure. The fact that all four methods produced the same northwest-southeast gravity gradient, even though they used different mathematical formulas, suggests that the regional structural trend is strongly expressed in the predictor variables, especially elevation and lithological density, and is not just a result of one modeling approach. This result has practical relevance for geodetic applications in Namibia, as it suggests that all four methods are capable of reproducing the primary regional gravity field structure. However, differences in model performance remain consequential at the short-wavelength scales that are critical for high-resolution geoid refinement and precise vertical datum modernization. This is because the systematic biases and localized overfitting tendencies identified in this study would propagate directly into geoid height errors if left unaddressed.

4.5.2 Difference analysis

The difference maps and residual distributions in Figure 7 reveal that GPR achieved the closest spatial agreement with Universal Kriging (RMSE difference = 8.48 mGal), with a near-symmetric, low-kurtosis residual distribution that indicates a stable prediction behaviour across the study area. This agrees with Moore et al. (2016), who demonstrated that the Matérn kernel GPR is effective at constraining spatial oscillations in data-sparse situations, and with Kaloop et al. (2022), who demonstrated that ML models that include terrain and geophysical predictors

consistently outperform purely geostatistical methods in regional gravity tasks. The most spatially heterogeneous residuals were produced by ANN, and the largest departure from Kriging was concentrated in the western high-anomaly domain, consistent with the overfitting tendency identified in the validation analysis and with Zhanakulova et al. (2025), who reported similar ANN instability under sparse training conditions.

SVM showed spatially uniform but persistently positive residuals (mean difference = +2.58 mGal). This reflects its conservative generalization behavior, which was also noted by Elshewy et al. (2024). Elshewy et al. (2024) had attributed a similarly comparable SVM bias to the margin penalty pulling predictions toward the central tendency of the training distribution. Critically, the broadly symmetric and near-normal residual distributions for all three ML models indicate that divergence from Universal Kriging is predominantly random rather than systematically directional. This supports the conclusion that all four methods capture the same underlying regional gravity field structure, with method-specific deviations in local spatial detail. The conclusion aligns with the emerging consensus that ML and geostatistical approaches are complementary rather than competing methodologies in regional gravity field modelling (Elshewy et al., 2024; Zhanakulova et al., 2025).

5. Conclusion

This study examined four predictive modeling techniques for high-resolution Bouguer gravity anomaly forecasting in the data-sparse Khomas Region of Namibia, utilizing terrestrial gravity observations combined with elevation, slope, and lithological density predictors. All four methods consistently replicated the prevailing northwest–southeast regional gravity gradient, validating that the principal large-scale signal is reliably retrievable across fundamentally distinct modeling frameworks under sparse observational conditions. A quantitative assessment using spatially distributed hold-out validation showed that GPR had the highest indicative accuracy (MAE = 4.67 mGal; RMSE = 5.33 mGal) and the best spatial agreement with Universal Kriging (r = 0.9073). The predictions were stable and stayed within physically plausible limits at both grid resolutions. ANN had the broadest dynamic range and was most sensitive to small changes in input, although it did overfit at small spatial scales. SVM, however, had the most conservative and resolution-independent outputs. Universal Kriging was able to reproduce the observed gravity field distribution accurately and is a reliable geostatistical baseline. However, its inability to integrate auxiliary predictors constrains its effectiveness in resolving physically motivated short-wavelength signals.

Despite the small validation sample, the comparison results provide useful information for gravity-based geodetic applications in Namibia. GPR is recommended for operational geoid refinement and vertical datum modernization efforts where prediction consistency, uncertainty quantification, and physical plausibility are critical. SVM and Universal Kriging are good options for characterizing the gravitational field on a regional scale because they are robust and do not require too much processing power. ANN may be better for fine-scale studies when there is enough training data to limit its high-frequency responses. The difference maps and residual analysis show that the model diverges from Universal Kriging mostly at random, not in a systematic way. The method-specific deviations are limited to short-wavelength spatial detail, which is still important for accurately determining the geoid. The approach and comparison benchmarks proposed herein serves as a foundational method for upgrading gravity fields, modernization of national vertical datum, and broader geodetic modernization initiatives throughout Namibia and similar data-sparse regions.

Conflict of Interest statement

The authors declare that there is no known financial, professional, or personal conflict of interest that could have influenced the results, interpretation, or presentation of this research.

Data Access Statement

This study used terrestrial Bouguer gravity anomaly data obtained from the Bureau Gravimétrique International (BGI), topographic data from the publicly available SRTM 30-m Digital Elevation Model, and geological density information derived from lithological maps sourced from the Ministry of Mines and Energy of Namibia. The BGI gravity dataset is accessible through the BGI portal (http://bgi.obs-mip.fr) upon registration. SRTM data are freely available from NASA/USGS repositories. Processed model outputs and derived datasets are available from the corresponding author upon reasonable request.

Ethics statement

This study is based on publicly available and institutionally sourced geospatial datasets including terrestrial gravity observations, remote sensing elevation data, and published geological maps. No human participants, animals, clinical data, or sensitive personal information were involved in this research. Therefore, institutional ethical approval was not required for this study.

Funding statement

This research received no specific grant from any funding agency in the public, commercial, or not-for-profit sectors. However, the authors acknowledge institutional support from colleagues at the the Department of Land and Spatial Sciences (Geomatics division), Namibia University of Science and Technology (NUST), Namibia.

References

Abd-Elmotaal, H., N. Kühtreiber, K. Seitz, and B. Heck. 2020. "A Precise Geoid Model for Africa: AFRgeo2019." *International Association of Geodesy Symposia*. https://doi.org/10.1007/1345_2020_122

Bašić, T., D. Markovinović, M. Varga, and O. Oršulić. 2019. "The Impact of Terrestrial Gravity Data Density on Geoid Accuracy: Case Study Bilogora, Croatia." *Survey Review* 52(373):299–308. https://doi.org/10.1080/00396265.2018.1562747

Blakely, R. J. 1995. *Potential Theory in Gravity and Magnetic Applications*. Cambridge: Cambridge University Press.

Burgess, T. M., and R. Webster. 2019. "Optimal Interpolation and Isarithmic Mapping of Soil Properties: I The Semi-variogram and Punctual Kriging." *European Journal of Soil Science* 70(1):11–19. https://doi.org/10.1111/ejss.12784

Darbeheshti, N., and W. E. Featherstone. 2009. "Non-Stationary Covariance Function Modelling in 2D Least-Squares Collocation." *Journal of Geodesy* 83:495–508. https://doi.org/10.1007/s00190-008-0267-0

Elshewy, M. A., P. T. Thanh, A. M. Elsheshtawy, M. Refaat, and M. Freeshah. 2024. "A Novel Approach for Optimizing Regional Geoid Modeling over Rugged Terrains Based on Global Geopotential Models and Artificial Intelligence Algorithms." *Egyptian Journal of Remote Sensing and Space Sciences* 27(4):656–668. https://doi.org/10.1016/j.ejrs.2024.09.002

Forsberg, R., and A. V. Olesen. 2010. "Airborne Gravity Field Determination." Pp. 83–104 in *Sciences of Geodesy I: Advances and Future Directions*, edited by G. Xu. Berlin: Springer.

Fusami, A. A., J. D. Edan, and A. Takana. 2023. "Local Orthometric Height Based on a Combination of GPS-Derived Ellipsoidal Height and Geoid Model: A Review Paper." *Journal of Geodetic Science* 13(1). https://doi.org/10.1515/jogs-2022-0158

Gruber, T., C. Gerlach, and R. Haagmans. 2012. "Intercontinental Height Datum Connection with GOCE and GPS-Levelling Data." *Journal of Geodetic Science* 2(4):270–280.

Harms, J. 2019. "Terrestrial Gravity Fluctuations." *Living Reviews in Relativity* 22 6. https://doi.org/10.1007/s41114-019-0022-2

Hirt, C., M. Yang, M. Kuhn, B. Bucha, A. Kurzmann, and R. Pail. 2019. "SRTM2gravity: An Ultrahigh Resolution Global Model of Gravimetric Terrain Corrections." *Geophysical Research Letters* 46. https://doi.org/10.1029/2019GL082521

Hu, B., J. Li, G. Su, J. Jiang, and J. Sheng. 2019. "Uncertain Prediction for Slope Displacement Time-Series Using Gaussian Process Machine Learning." *IEEE Access* 7:27535–27546. https://doi.org/10.1109/access.2019.2894807

Ihde, J., L. Sánchez, R. Barzaghi, H. Drewes, C. Foerste, T. Gruber, G. Liebsch, U. Marti, R. Pail, and M. Sideris. 2017. "Definition and Proposed Realization of the International Height Reference System (IHRS)." *Surveys in Geophysics* 38(3):549–570.

Ikirri, M., M. Jaffal, I. Rezouki, F. Z. Echogdali, S. Boutaleb, K. Abdelrahman, T. Abu-Alam, F. Faik, A. Kchikach, and M. Abioui. 2023. "Contribution of Gravity Data for Structural Characterization of the Ifni Inlier, Western Anti-Atlas, Morocco: Hydrogeological Implications." *Applied Sciences* 13:6002. https://doi.org/10.3390/app13106002

Jiang, T., Y. Dang, and C. Zhang. 2020. "Gravimetric Geoid Modeling from the Combination of Satellite Gravity Model, Terrestrial and Airborne Gravity Data: A Case Study in the Mountainous Area, Colorado." *Earth, Planets and Space* 72:189. https://doi.org/10.1186/s40623-020-01287-y

Kaloop, M. R., S. Pijush, M. Rabah, H. Al-Ajami, J. W. Hu, and A. Zaki. 2022. "Improving Accuracy of Local Geoid Model Using Machine Learning Approaches and Residuals of GPS/Levelling Geoid Height." *Survey Review* 54(387):505–518. https://doi.org/10.1080/00396265.2021.1970918

Liu, Q., M. Schmidt, L. Sánchez, L. Moisés, and D. Cortez. 2024. "High-Resolution Regional Gravity Field Modeling in Data-Challenging Regions for the Realization of Geopotential-Based Height Systems." *Earth, Planets and Space* 76:35. https://doi.org/10.1186/s40623-024-01981-1

Lloyd, C., and P. Atkinson. 2002. "Non-Stationary Approaches for Mapping Terrain and Assessing Prediction Uncertainty." *Transactions in GIS* 6:17–30. https://doi.org/10.1111/1467-9671.00092

Miky, Y. H., R. Yaagoubi, and A. El Shouny. 2017. "Study of the Potential of a Local Geoid Model for Extracting the Orthometric Heights from GPS Measurements in Topographic Works." *Civil and Environmental Research* 9(7):16–28.

Moore, C. J., J. R. Gair, C. P. L. Berry, and A. J. K. Chua. 2016. "Fast Methods for Training Gaussian Processes on Large Datasets." *Royal Society Open Science* 3(5):160125. https://doi.org/10.1098/rsos.160125

Odumosu, J. O., and V. C. Nnam. 2020. "Gravity Data Requirements for Decimetre Accuracy Regional Geoid Using Stokes' Remove Compute Restore Technique in Nigeria." *Contributions to Geophysics and Geodesy* 50(3). https://doi.org/10.31577/congeo.2020.50.3.3

Odumosu, J. O., V. C. Nnam, and I. J. Nwadialor. 2021. "An Assessment of Spatial Methods for Merging Terrestrial with GGM-Derived Gravity Anomaly Data." *Journal of African Earth Sciences* 104202.

Peprah, M. S., A. Odoom, E. K. Larbi, and M. A. Mwin. 2026. "A Comparative Analysis of Random Forest and Gradient Boosting Regression Techniques in Google Colab for Air Temperature Prediction in the Greater Accra Region, Ghana." *Journal of Geomatics* 20(1):55–60. https://doi.org/10.58825/jog.2026.20.1.259

Sobrero, F. S., K. Ahlgren, M. G. Bevis, D. D. Gómez, J. Heck, A. Echalar, E. Kendrik, P. Montenegro, A. Batisti, J. C. Catari, R. T. Sallici, and H. G. Trigo. 2024. "A Robust Approach to Terrestrial Relative Gravity Measurements and Adjustment of Gravity Networks." *Journal of Geodesy* 98:86. https://doi.org/10.1007/s00190-024-01891-w

Warren, S. D., M. G. Hohmann, K. Auerswald, and H. Mitasova. 2004. "An Evaluation of Methods to Determine Slope Using Digital Elevation Data." *CATENA* 58(3):215–233. https://doi.org/10.1016/j.catena.2004.05.001

Xiong, L., S. Li, G. Tang, and J. Strobl. 2022. "Geomorphometry and Terrain Analysis: Data, Methods, Platforms and Applications." *Earth-Science Reviews* 233:104191. https://doi.org/10.1016/j.earscirev.2022.104191

Zhanakulova, K., B. Adebiyet, E. Orynbassarova, A. Yerzhankyzy, K.-K. Kassymkanova, R. Abdykalykova, and M. Zakariya. 2025. "Application of Machine Learning Methods for Gravity Anomaly Prediction." *Geosciences* 15(5):175.